PCCP

PAPER

Magnesia-stabilised zirconia solid electrolyte assisted electrochemical investigation of iron ions in the SiO_2-CaO-MgO-Al_2O_3 molten slag at 1723 K

Received 27th March 2017,
Accepted 00th xx 2017

DOI: 10.1039/x0xx00000x

www.rsc.org/

Yunming Gao,*[ab] Chuanghuang Yang,[ab] Canlei Zhang,[ab] Qingwei Qin[ab] and George Z. Chen[abc]

Production of metallic iron through molten oxide electrolysis using inert electrodes is an alternative route for fast ironmaking without CO_2 emissions. The fact that many inorganic oxides melt at ultrahigh temperatures (>1500 K) challenges conventional electro-analytical techniques used in aqueous, organic and molten salt electrolytes. However, in order to design a feasible and effective electrolytic process, it is necessary to best understand the electrochemical properties of iron ions in molten oxide electrolytes. In this work, a magnesia-stabilised zirconia (MSZ) tube with a closed end was used to construct an integrated three-electrode cell with the "MSZ | Pt | O_2 (air)" assembly functioning as the solid electrolyte, the reference electrode and also the counter electrode. Electrochemical reduction of iron ions was systematically investigated on an iridium (Ir) wire working electrode in the SiO_2-CaO-MgO-Al_2O_3 molten slag at 1723 K by cyclic voltammetry (CV), square wave voltammetry (SWV), chronopotentiometry (CP) and potentiostatic electrolysis (PE). The results show that the electroreduction of the Fe^{2+} ion to Fe on the Ir electrode in the molten slag follows a single two-electron transfer step, and the rate of the process is diffusion controlled. The peak current on the obtained CVs is proportional to the concentration of the Fe^{2+} ion in the molten slag and the square root of scan rate. The diffusion coefficient of Fe^{2+} ions in the molten slag containing 5 wt% FeO at 1723 K was derived to be $(3.43 \pm 0.06)\times10^{-6}$ cm^2 s^{-1} from CP analysis. However, a couple of following processes, i.e. alloy formation on the Ir electrode surface and interdiffusion were found to affect the kinetics of iron deposition. An ECC mechanism is proposed to account for the CV observations. The findings from this work confirm that zirconia-based solid electrolytes can play an important role in electrochemical fundamental research in high temperature molten slag electrolytes.

1. Introduction

Amongst all metallic materials used by human beings, iron and steel are the most important base materials with maximum quantities of usage and the widest range of application. Currently, iron is produced almost exclusively through reduction of iron ores by carbon (coke) in the blast furnace. Iron cannot be converted into steel until excessive impurities contained in iron, such as carbon, silicon, manganese, sulphur and phosphorus, are removed. Consequently, the smelting process for the production of iron and steel becomes longer, resulting in a series of problems, such as high-energy consumption, low efficient utilisation and environment pollution. Specifically, it is estimated that the carbothermic reduction process that is dominant in the current industry for the production of iron and steel contributes to about 5% of the total global anthropogenic CO_2 emissions.[1] Hence, the current steelmaking industry faces difficult environmental challenges. For this reason, the ultra-low CO_2 steelmaking (ULCOS) program has been set up in Europe with the aim to develop four breakthrough technologies that are expected to drastically reduce greenhouse gas emissions.[2] Electrolytic production, as one of the four technologies, has drawn increasing attention along with the development of renewable electricity in recent years. Coupled with an inert anode, it can obtain carbon-free iron, shorten the smelting process, and also eliminate the CO_2 emissions. Electrolytic production of iron can be carried out in molten salts and has proven to be promising in laboratory.[3-9] In particular, molten oxide electrolysis (MOE) developed by Sadoway and co-workers,[3,4] which can directly produce carbon-free liquid iron along with the oxygen gas, is expected to be an alternative compact process that exhibits exceptionally high productivity in comparison with other electrowinning techniques.[6,7] It is even considered for producing oxygen from lunar or Martian regolith in space exploration. [5]

Generally, iron oxide dissolved in a molten slag is in the forms of iron cations (Fe^{3+} and Fe^{2+}) and oxygen anion (O^{2-}). During MOE, the iron ions are reduced on the cathode and metallic iron or a ferroalloy is obtained, while O^{2-} is oxidised on the anode to emit the oxygen gas which is beneficial to the natural conversion of CO_2 back to carbon or hydrocarbons. In order to design an effective,

[a] The State Key Laboratory of Refractories and Metallurgy, Wuhan University of Science and Technology, Wuhan 430081, China.
[b] Key Laboratory for Ferrous Metallurgy and Resources Utilization of Ministry of Education, Wuhan University of Science and Technology, Wuhan 430081, China.
E-mail: gaoyunming@wust.edu.cn
[c] Department of Chemical and Environmental Engineering, Faculty of Engineering, University of Nottingham, Nottingham NG7 2RD, UK.

commercially feasible and green electrolytic process, it is necessary and crucial to best understand the chemical and electrochemical behaviour of iron ions in molten slag at high temperatures.

Generally, most inorganic oxides that are needed for MOE can only melt at ultrahigh temperatures (>1500 K). For example, the melting points of the commonly used SiO_2, Al_2O_3, CaO and MgO are 1986, 2345, 2886, and 3125 K, respectively. Mixing these oxides to an appropriate composition can have a certain effect in reducing the melting temperature which however often remains higher than 1500 K. This fact challenges investigation of electrochemical behaviour of active species in conventional three-electrode cells for aqueous, organic or molten salt electrolytes. This is because ultrahigh temperatures not only compromise the material stability of the electrodes (especially reference electrode) and the cells, but also enhance interferences from non-oxide impurities, leading to, for example, intrinsic electronic conductivity through the molten electrolyte.[10] Moreover, in order to prevent interactions between species produced from reactions on the anode and cathode, it is necessary to use a separation membrane that is conducting to selected ions (of the electrolyte components) but nothing else. Unfortunately, it is also very difficult to choose such membrane materials for service at ultrahigh temperatures. These ultrahigh temperatures not only lead to difficulties for electrochemical analyses (the higher the temperature, the more difficult the operation), but may also cause an unfavourable impact on the reproducibility and reliability of the experimental results.

To our knowledge, with the aid of traditional three-electrode cells, a few studies have been conducted on electrochemical behaviour of iron ions at high temperatures.[11-22] Most of these were performed in various molten salts at temperatures lower than 1273 K.[11-15] Furthermore, the research findings were sometime inconsistent under different test conditions. For instance, the reduction of Fe^{2+} to Fe was considered to be a reversible process by Duan *et al*[11] and Chryssoulakis *et al*,[12] quasi-reversible by Castrillejo *et al*,[13] but irreversible by Lugovskoy *et al*[14] and Donath *et al*.[15] Although some investigations were performed in molten slags (mainly glass melts), most of these were limited to the Fe^{3+}/Fe^{2+} redox couple by a single electrochemical technique, and evaded the Fe^{2+}/Fe redox couple.[16-22] Specifically, the reduction of Fe^{2+} to Fe in glass melts at 1473 K was only reported as an irreversible process by Strycker *et al*,[17] but they did not give further information on the reduction of ferrous ions. Wang *et al*[4] pioneered a voltammetric study of iron deposition in a Mo crucible using Mo rods as the working, reference and counter electrodes in the molten slag of SiO_2 (49 wt%), CaO (25 wt%), and MgO (26 wt%) at 1848 K. They have observed current peaks of the Fe^{2+}/Fe couple on cyclic voltammograms (CVs). This finding is unprecedented and calls for further analyses of the electrode reaction mechanism in ultrahigh temperature molten slags. It is obviously necessary to establish a feasible experimental protocol for systematic electrochemical analyses of iron ions at ultrahigh temperatures.

The recent investigation by Wang *et al*[4] indicates that the SiO_2-CaO-MgO-Al_2O_3 slag is a potential medium for electrolytic extraction of liquid iron. In this work, we aim to demonstrate a unique integrated three-electrode cell for fundamental investigation of the electrochemical properties of iron ions in a mixed SiO_2-CaO-MgO-Al_2O_3 molten slag at 1723 K. For this purpose, a zirconia based solid oxide electrolyte has been selected as the material for making both the oxygen-ion conducting membrane and cell container. It is well known that zirconia doped with magnesia (MgO) or yttria (Y_2O_3) has highly selective oxygen ionic conductivity, low electronic conductivity and strong corrosion resistance in high temperature media. These zirconia-based solid electrolytes have been widely used not only in metallurgical industry, but also fundamental research,[23-36] including determination of activity[23,24] and diffusion coefficient[25,26] of oxygen in metal melt, determination of activity of FeO in molten slag,[27,28] electrolytic refining of metal melt,[29,30] and extraction of metal from dissolved oxide in molten salt or molten slag.[31-33] In this work, a magnesia-stabilised zirconia (MSZ) solid electrolyte tube was used to accommodate the SiO_2-CaO-MgO-Al_2O_3 molten slag containing FeO. Electrochemical behaviour of iron ions in the molten slag at 1723 K was investigated by combining with a variety of electrochemical means, including CV, square wave voltammetry (SWV), chronopotentiometry (CP), and potentiostatic electrolysis (PE).

This work is a part of a systematic research programme focused on green electrolytic process associated with steelmaking. It is expected to provide a theoretical basis for electrolytic extraction of iron from molten slag without emission of CO_2. The MSZ tube has been employed for multiple purposes in this work. It serves as the container of the molten slag, oxide ion conducting membrane to physically separate the working electrode (WE) and the counter electrode (CE). It also provides a basal body integrating a CE with a stable "MSZ | Pt | O_2 (air)" reference electrode (RE) (in fact an "O^{2-}|O_2" RE). Therefore, this work also aims to demonstrate that zirconia-based solid electrolytes can play an important role in electrochemical fundamental research on molten slag electrolytes at ultrahigh temperatures. At present, a few researchers are trying to develop a new non-metallic anode for MOE.[3,9] In this line, this work offers a research direction to the development of the potential zirconia based inert anodes.

2. Experimental

2.1. Preparation of synthetic slags

The mother slag for the experiments was prepared from $CaCO_3$, SiO_2, Al_2O_3 and MgO (analytical reagent (AR) grade in purity) that were uniformly mixed in the base composition of 47 wt% SiO_2, 28 wt% CaO, 16 wt% MgO, and 9 wt% Al_2O_3. The mixture was then calcined at 1223 K for 6 h in a muffle furnace. At room temperature, the CaO reagent stored for a long time may deteriorate due to damp, and the CaO activity becomes poor. Here pure CaO with a good reaction activity can be obtained by the decomposition of $CaCO_3$ at high temperature. The practice of replacing CaO with $CaCO_3$ can be found in metallurgical experiments.[18,37-40]. FeO in the form of the ferrous oxalate (AR) powder was directly added into the mother slag.[22] The above mixed powders were poured into an alumina crucible with high purity of 99.5 wt% Al_2O_3. The crucible was positioned in a vertical tube furnace with the $MoSi_2$ heating elements. The chamber of the furnace was flushed with argon that was purified successively in a two-stage treatment of copper wires and magnesium chips at 853 K. The furnace was programmed to heat to

1623 K, and held at this temperature for 1 h to melt the slag. In order to obtain a homogeneous melt, the slag was agitated with a thin alumina rod for 5 min. once every 15 min. at the holding temperature. Subsequently, the crucible containing the slag melt was removed rapidly from the furnace chamber and then quenched in a large amount of water. The practice of quenching slag melt containing iron oxide in water can be found in literature.[40-42] Although the alumina crucible might crack in the water, the slag almost remained intact after solidification. The slag could be taken out from the water and separated from the crucible. After drying, the quenched slag was ground in an agate mill, collected and stored in a drying desiccator before further uses.

2.2. Construction of the integrated cell

The integrated three-electrode cell was fabricated from of an MSZ tube with a closed end as schematically illustrated in Fig. 1. The MSZ tube was 7.3 mm in inner diameter, 10.0 mm in outer diameter and 79.0 mm in length, and contained 2.18 wt% MgO (supplied by University of Science & Technology Beijing, China). Platinum (Pt) paste (supplied by Sino-Platinum Metals Co., Ltd, China) was uniformly painted on two adjacent small areas of the outer surface of the MSZ tube near the closed end to form two porous Pt electrodes. The Pt painted MSZ tube was dried in air, and then placed in the muffle furnace to sinter in air for 30 min at 1173 K. Afterwards, the two porous Pt electrodes coated on the MSZ tube were subjected to conductivity and scratch tests, and it was found that resistance between any two points in each Pt coated area was less than 0.2 Ω. The manual scratch tests confirmed the Pt coatings to be uniform with strong adhesion on to the outer surface of the MSZ tube. The Pt coating near the closed bottom was used as the "MSZ | Pt | O_2 (air)" RE (1.57 cm^2 in area), the other as the CE (1.26 cm^2 in area). The leads of the RE and CE were Pt wires (0.5 mm in diameter). Approximately 1.5 g slag prepared as described above was loaded inside the MSZ tube for each test.

A crucial part of this study was to select a sufficiently inert WE suitable for electro-deposition of Fe in molten slags. Nearly all solid metal electrodes can alloy with iron at a high enough temperature (e.g. 1723 K). Generally Mo and metals of the Pt family (including Pt, Ir) are often used for making the WE, but these metals can easily alloy with Fe at higher temperatures. Mo is also susceptible to oxidation, even by iron oxide in molten slag. Obviously Mo is not suitable for use in this work. Pure Fe has a melting point (1811 K) that is close to the molten slag temperature (1723 K). Therefore, a thin Fe wire would be too soft at our working temperature to enable reliable insertion of the wire into the viscous molten slag without deformation of the wire. Use of a thicker Fe wire introduces inevitably a larger electrode surface area, leading to very large currents (> 1 A) from the reduction and the re-oxidation. This in turn would not only cause a non-negligible change of the concentration of iron oxide in the molten slag, but also increase deviation from the applied *IR* (*I*: current; *R*: resistance) drop compensation, leading to experimental results with poor stability and reproducibility. More adversely, iron oxides can easily form on the Fe surface under our experimental conditions, and hence interfere with the analysis of the iron ions in the molten slag. Therefore, pure Fe was not selected in this work.

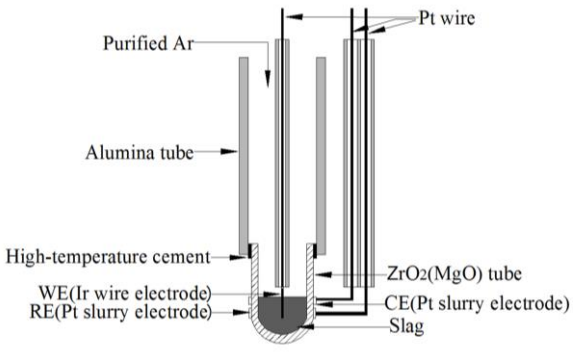

Fig. 1 Schematic illustration of the MSZ based integrated three electrode cell for electrochemical analyses in molten slags at ultrahigh temperatures (1723 K in this work).

Pt possesses higher oxidation resistance and better chemical stability, but a thin Pt wire, although better than the Fe thin wire, also becomes too soft to retain its shape at higher temperatures, which is unfavourable for the insertion operation. Thus, Pt was not selected in this work, either.

Ir is similar to Pt in many aspects, whilst thermodynamic calculations show that Ir oxides (e.g. IrO_2), if formed, can decompose spontaneously at higher temperatures, and will not affect the use of Ir as a metal electrode. Gmitter[43] made a detailed discussion on stability of Ir oxides in his thesis where Ir wire was used as the working electrode in the positive potential range. It was believed that the formed IrO_2 decomposed rapidly into Ir and oxygen and did not dissolve in the molten electrolyte. Wang' work[4] in laboratory demonstrated that Ir could serve as an oxygen-evolving inert anode in molten oxide electrolysis. However, it should be noted that oxidation of Ir in the molten slag proceeds only in the positive potential range. This can also be inferred from the following CV curve of blank slag with scan in the negative direction where no oxidation peak of Ir is observed in this work. Since the present work deals mainly with the reduction of iron ions in the negative potential range, no oxidation of Ir is actually involved in this work. Most importantly, Ir possesses higher melting point (2719 K) and mechanical strength (528 GPa) than Pt (2041 K, 168 GPa), and is more favourable for the insertion operation in this work. Therefore, Ir was considered the more suitable WE material in this work. One end of the Ir wire (0.5 mm in diameter, 30 mm in length, purity at 99.95 wt%) was inserted into the molten slag and the other end was connected to a Pt wire (0.5 mm in diameter) served as the current lead. All Pt wires as the electrode leads were protected within thin alumina tubes.

2.3. Experimental methods

The integrated three-electrode cell as shown in Fig. 1 was used for all electrochemical measurements which were controlled by a CHI1140A electrochemical workstation (supplied by Shanghai CH Instruments Co., Ltd, China) coupled with the software and a computer for data collection and storage. For easy operation, the open end of MSZ tube was connected to an alumina tube with a high-temperature cement. The cell unit was positioned in the constant temperature zone of the vertical tube furnace. The dried

argon purified in the manner mentioned above was introduced into the furnace chamber and the MSZ tube at a flow rate of 400 and 20 mL min^{-1}, respectively. It should be emphasized that the inside diameter of the furnace tube is relatively thin with only 30 mm and the gas is introduced into the furnace chamber from bottom to top, which are helpful to the rapid replacement of gas. A Pt-Rh (6 wt%) | Pt-Rh (30 wt%) thermocouple (Type B) was employed to determine the experimental temperature. The furnace was programmed to heat to 1723 K at a rate of 5 K min^{-1} and held the temperature constant for at least 30 min. While holding the temperature, the Ir WE was slowly inserted into the molten slag carefully to avoid any contact with the inner wall of the MSZ tube. The exact contact point between the electrode and the surface of molten slag was determined by observing the sudden change on the open-circuit potential (OCP) *vs* time curve recorded in real-time. Fig. 2 shows a typical OCP – time curve in the course of immersing the Ir wire into the molten slag containing 3 wt% FeO. Note that all potentials in this work were reported with reference to the "MSZ | Pt | O_2 (air)" RE.

In order to ensure the comparability of the results (especially in current density) of each test, taking into account the control accuracy of insertion depth of the WE, it is necessary to select first the insertion depth which has the least influence on the current density as the uniform depth of all subsequent tests. In this way, the influence of the possible deviation of insertion depth of the electrode on the current density can be reduced. Fig. 3a presented CVs recorded for molten slag containing 5 wt% FeO at different immersion depths of the Ir wire WE into the molten slag in preliminary experiments. It showed that the current changed constantly with the immersion depth; however, the corresponding current density (*j*) changed little after the immersion depth reached 9 mm, as shown in Fig. 3b. Thus it was determined that in each experiment the immersion depth of the WE into the molten slag was 9 mm (corresponding to a contacting area of 0.1413 cm^2 with the molten slag), so as to avoid the influence of the difference of immersion depth of the WE on electrochemical signal. Finally, the Ar atmosphere in the furnace chamber was switched to dry air with a flow rate at 400 mL min^{-1} to constitute the RE with stable oxygen partial pressure outside the MSZ tube. A quick response of the OCP was observed during the switch, as shown in Fig. 2. Under the air condition, the OCP became stable after a few minutes when it was considered to be suitable for electrochemical experiments.

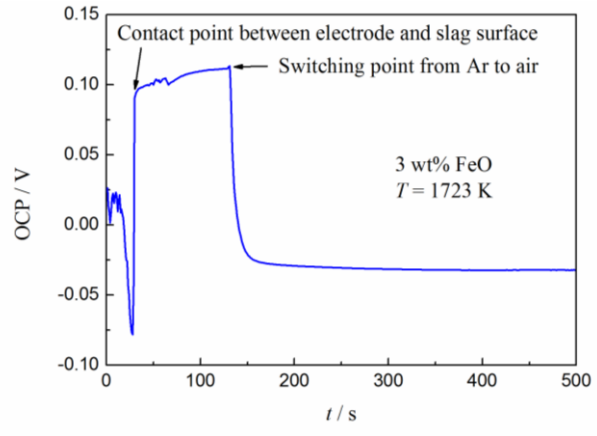

Fig. 2 A typical OCP – time curve recorded in the course of immersing the Ir wire WE into the molten slag containing 3 wt% FeO and then switching from Ar to dry air in the furnace chamber. The OCP was measured against the "MSZ | Pt | O_2 (air)" RE after switching from Ar to air.

CV, SWV, CP and PE were employed in the experiment. Positive feedback for 100 % *IR* drop compensation was applied in CV and SWVs, but not in CP because the workstation did not support the same. In this work, the OCP – time curve was repeatedly measured to determine the stable OCP prior to next measurement, unless otherwise stated. It was found that the differences between all measured stable OCP were within 20 mV which was considered as evidence of the cell being in the same quasi-stable state prior to each measurement.

In addition, the molten slags containing 3 wt% FeO were electrolyzed for 2 h at constant potentials of -0.40, -1.00, -1.30 V, respectively. The structural features and the morphology of the residues were characterised by scanning electron microscope (SEM) (Nova 400 Nano) and the energy dispersive X-ray spectrometer

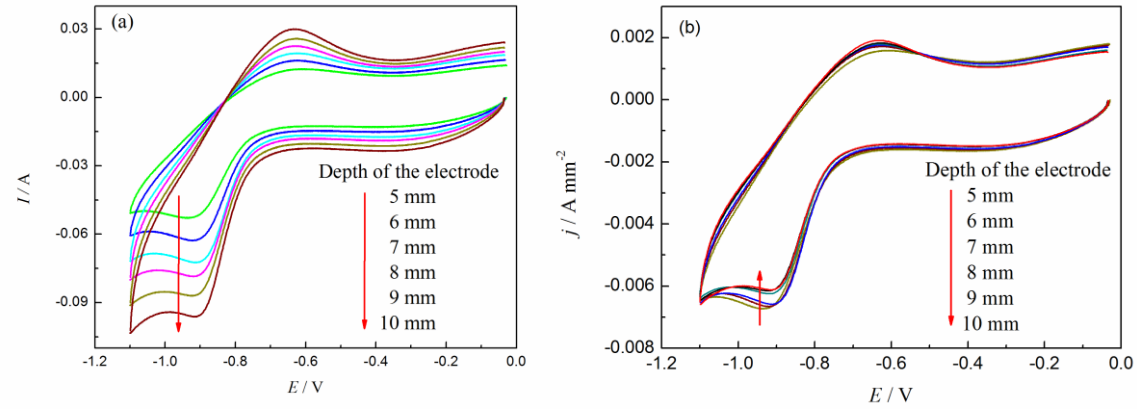

Fig. 3 (a) Cyclic voltammograms recorded in the molten slag containing 5 wt% FeO at different immersion depths of the Ir wire WE under dry air; (b) The corresponding current density (*j*) at different immersion depths of the Ir wire WE. RE: MSZ | Pt | O_2 (air). Temperature: 1723 K. Scan rate: 0.2 V s^{-1}.

(EDS) (INCAIE 350 Penta FET X-3). Here, the Ir wire is selected as the cathode and the main purpose is to maintain a consistency with the Ir wire used as the WE for the investigation of Fe^{2+} reduction behaviour so as to verify the reduced product in CV tests. Obviously, instead of Ir, Fe or steel will be the more affordable choice in the real industrial electrolysis.

2.4. Methods of calculation

For reference in the analyses of electrochemical test results, the theoretical decomposition potential of oxide components, as well as the composition of gas-liquid-solid equilibrium in the system was calculated using the Factsage thermodynamic software,[44,45] assuming an oxygen partial pressure of 21 kPa (the same oxygen partial pressure of the air reference state in the experiment), and a unity activity of the metal product (M) from corresponding reduction process. The decomposition reaction of oxide (M_xO_y) in the molten slag can be described by the following reaction.

$$M_xO_y = x\ M + y/2\ O_2 \quad (1)$$

In particular,

$$Fe_2O_3 = 2\ FeO + ½\ O_2 \quad (2)$$

Because the RE used in this work is the $O^{2-}|O_2$ couple in nature, the decomposition potential of the oxide is in value equal to the onset reduction potential of corresponding active ions in an ideal case.

3. Results and discussion

3.1. Basic considerations

Determination of potential scan range. In order to determine suitable scan potential range, CV technique was first employed. Fig. 4 shows the CVs recorded in the molten slag with different FeO concentrations at typical scan rate of 0.2 Vs^{-1}. In the absence of FeO, the CV (Blank slag in Fig. 4) exhibits minimum currents close to zero with minor change in the potential range of 0 to -1.20 V. This is evidence of no electrochemical reaction occurs, indicating negligible redox active impurities and good electrochemical stability of both the blank slag and the WE in this potential range. When the negative scan runs beyond -1.20 V, a cathodic peak (C_1) appears at -1.30 V and the corresponding anodic peak (A_1) is observed at -1.15 V upon reversing the scan. The theoretical calculations from Factsage thermodynamics software indicate that SiO_2 is the easiest to reduce in the blank slag. Thus, C_1/A_1 can be attributed to the Si^{4+}/Si redox couple. According to the Ir-Si phase diagram,[46] the reduced silicon and the Ir are likely to form an alloy with a lower melting point, which leads to the potential interference to reduction of iron ions and the damage of the Ir electrode. Therefore, it is necessary to ensure that the potential scan is limited in a range to avoid the reduction of Si^{4+} but allows the full reduction of Fe^{2+} as shown in Fig. 4.

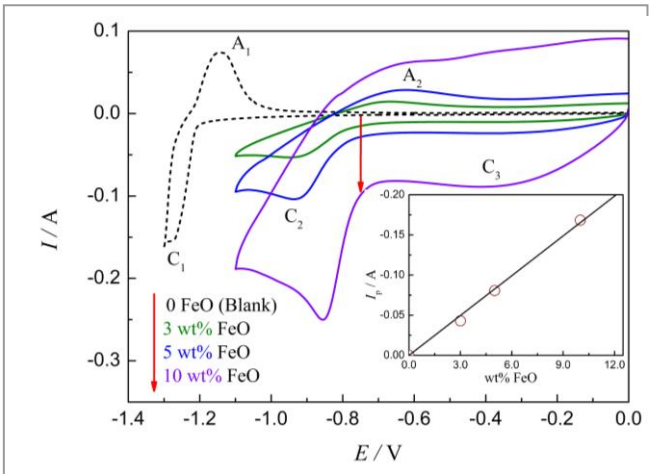

Fig. 4 CVs recorded in the molten slag with different FeO concentrations. Inset: The correlation between the cathodic peak current (I_p) and the FeO concentration (wt% FeO). Temperature: 1723 K. Scan rate: 0.2 V s^{-1}. RE: MSZ | Pt | O_2 (air).

In comparison with the CV of the blank slag, addition of FeO leads to a vague current peak C_3 between 0 and -0.7 V in Fig. 4. When the scan runs into the range of -0.7 to -1.1 V, a new and obvious pair of peaks (C_2/A_2) appears. After the deduction of the effect of background current, the current of peak C_2 linearly depends on the FeO concentration and the straight line passes through the origin[47] as shown in the inset of Fig. 4. Consequently, the C_2/A_2 can be associated to the Fe^{2+}/Fe couple, and the scan potential range may tentatively be set between 0 and -1.1 V.

In addition, it can be observed that the current becomes larger with increasing the FeO concentration to 10 wt%. Here the larger current means that not only the current of the reduction peak C_2 but also the background current increases. Too large a peak current is generally accompanied by a large charging current[48], and will also lead to inaccurate *IR* drop compensation and possibly a change in the morphology of the reduction product.This is not helpful to the analysis of electrochemical behaviour in the molten slag. Therefore, the molten slag containing 10 wt% FeO is not considered in this work. A detailed discussion on the main electrochemical characteristics of peak C_2 for the molten slag containing 5 wt% FeO will be carried out later in Section 3.2.

Confirmation of the reduction peak and the product morphology. Iron oxides mainly include Fe_2O_3 and FeO. However Fe_2O_3 is highly unstable at higher temperatures and can be decomposed into FeO and O_2 under certain conditions according to reaction (2). In a real industrial electrolysis for iron production, iron ore will be used as the raw material. It is well known that iron ore is predominantly ferric in nature. However for a molten slag containing iron oxide at higher temperatures, whether the original iron oxide is Fe_2O_3 or FeO, an equilibrium between Fe^{2+} and Fe^{3+}, and physically dissolved oxygen may be formed and represented by reaction (2') below:[17,20,49]

$$2\ Fe^{3+} + O^{2-} = 2\ Fe^{2+} + 1/2\ O_2 \quad (2')$$

Therefore, in this work, when the potential is scanned from 0 to -0.7 V in the negative direction, there may also be the reductions of the dissolved oxygen and/or Fe^{3+} ions in the molten slag although FeO is directly added into the slag in the form of ferrous oxalate. Thus, ill-defined peak C_3 can be attributed to the reduction of the dissolved oxygen or Fe^{3+} ions. This is one reason why the slag with addition of FeO has a larger current compared with the blank slag between 0 and -0.7 V in Fig. 4. Another reason could be an increase

in the background current. Here the background current mainly refers to charging current of the double layer since the redox of active impurities is negligible. It is well known that the total charging current of the double layer can be generated by the changing electrode potential and the melt composition variation. In Fig. 4, the charging current of the double layer from the change of the electrode potential always exists and remains constant at the same scan rate. Meanwhile, the charging current from the change of the double layer capacitance increases due to the increase of FeO concentration in the molten slag. Prange *et al*[48] found that the Fe electrode capacitance increased approximately linearly with the square root of the Fe^{2+} concentration in the CaF_2-FeO melt. Consequently the total charging current increases with the increase of FeO concentration in this work. Therefore, not only the current of the reduction peaks (C_2 and C_3) but also the total charging current increases with the increase in FeO concentration in the slag. Previous investigations[19,20,50] on the redox equilibrium between Fe^{2+} and Fe^{3+} in molten slag have indicated that the Fe^{2+}/Fe^{3+} molar ratio varies with the temperature, composition (particularly basicity) and oxygen partial pressure of the molten slag. It should be noted that the concentrations of Fe^{3+} and the dissolved oxygen in the molten slag are very small under Ar with a very low partial pressure of oxygen.[51-53] This results in a small current for the reduction peak C_3. In addition, it is known that the CV has a limited detection limit and larger error margins due to several factors, including charging current of the double layer mentioned above and the electronic current through the cell. It is reported that the molten slag containing FeO has an increased electronic conductivity.[10] These factors can make it difficult to observe the reduction peak C_3 with small current. This is one reason why the observed peak C_3 is not well-defined as shown in Fig. 4. Since the reduction potential for Fe^{3+} is close to that for the dissolved oxygen, it is difficult to use only CV to resolve these electrode processes in the molten slag.[18]

In order to judge whether there was the reduction of the dissolved oxygen and/or Fe^{3+} ions between 0 and -0.7 V, SWV was used in conjunction with PE. An attempt to change artificially the concentration of dissolved oxygen and/or Fe^{3+} in the molten slag was made by PE. SWVs of the molten slag containing 5 wt% FeO were measured and contrasted before and after PE. According to thermodynamic calculations,[44] the theoretical decomposition potentials of Fe_2O_3 and IrO_2 in the molten slag are -0.39 V and 0.11 V at 1723 K, respectively. Therefore, the applied constant potentials for electrolysis were set at -0.30 V and 0.10 V, respectively. It was reported[54] that the potential of the O_2/O^{2-} couple is more positive than that of Fe^{3+}/Fe^{2+} in glass melts. Thus, it is reasonable to expect that PE at -0.30 V may remove the dissolved oxygen from the molten slag regardless of the reduction of Fe^{3+} ions, while PE at 0.10 V may cause the oxidation of Fe^{2+} to Fe^{3+} in the molten slag, but neither the Ir electrode is oxidised nor is oxygen molecule formed. Thus, after the molten slag was in sequence electrolysed for 1.0 h at -0.30 V and 0.10 V, respectively, the amount of dissolved oxygen in the molten slag would most likely fall and of the Fe^{3+} ions rise. Subsequently measured SWVs were shown in Fig. 5.

In comparison with CVs in Fig. 4, a common reduction peak C_2 appears at -0.90 V in Fig. 5. Besides, a more prominent and narrower reduction peak C_3 arises at -0.10 V either before or after the PE, in

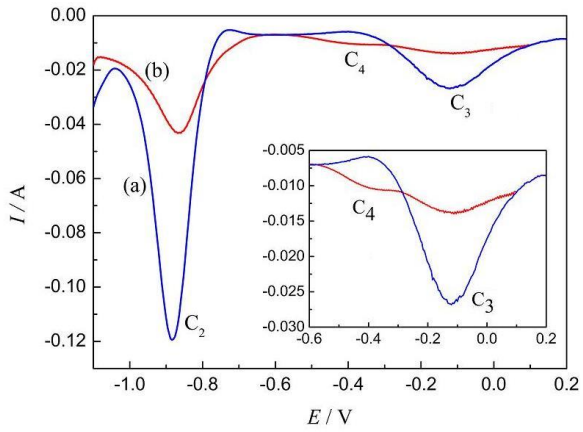

Fig. 5 SWVs recorded in the molten slag containing 5 wt% FeO at 1723 K, (a, blue line) 25 Hz, before PE; (b, red line) 20 Hz, after PE for 1 h at -0.3 V and 0.1 V, respectively. Inset: the magnified portion of peaks C_3 and C_4. RE: MSZ | Pt | O_2 (air).

contrast to the broad peak C_3 between 0 and -0.70 V on the CV in Fig. 4. A new reduction peak C_4 arises at -0.40 V on the SWV after the PE. The potential of peak C_2 is close to the theoretical decomposition potential of FeO (-0.80 V). Thus, peak C_2 can be attributed to the reaction: $Fe^{2+} + 2e \rightarrow Fe$. Some fluctuations can be observed on the magnified peak C_3 in the inset of Fig. 5, indicating gas involved in electrode reaction. This is related to the reduction of the dissolved oxygen: $1/2O_2 + 2e \rightarrow O^{2-}$. Both Nagata[18] and Gmitter[43] also reported that the reduction of the dissolved oxygen in the molten slag containing iron oxide could be observed during negative scan. The potential of peak C_4 is close to the theoretical decomposition potential of Fe_2O_3 (-0.39 V) and it can be attributed to the reaction, $Fe^{3+} + e \rightarrow Fe^{2+}$. The detected Fe^{3+} ions come from PE at 0.10 V which causes the oxidation of Fe^{2+} to Fe^{3+} in the molten slag. It is worth noting that the theoretical difference in decomposition potential between FeO and Fe_2O_3 is about -0.80 V - (-0.39 V) = -0.41 V relative to the same $O^{2-}|O_2$ RE. The value can be used for the purpose of comparison with the difference between peak potentials. It was found that the difference in peak potential between C_2 and C_4 is -0.90 V - (-0.40 V) = -0.50 V, but that between C_2 and C_3 is -0.90 V - (-0.10 V) = -0.80 V in Fig. 5. The former is much closer to the theoretical difference in decomposition potential (-0.41 V) between FeO and Fe_2O_3 than the latter, which further confirms the ownership of the above peaks. Note that the potential in SWV is stepped positively and negatively in alternation, which helps to cancel capacitive charging current. This is the reason why SWV has a better sensitivity and higher resolution than CV.

Despite of the PE, the peak C_3 still appears, indicating it is difficult to electrolytically remove the dissolved oxygen completely from the molten slag. This may be related to the viscosity of slag. No visible reduction of Fe^{3+} (peak C_4) is observed on the SWV of the original molten slag before the PE. Contrastively, the peak C_4 arises after the PE, and the peak current is much smaller than that of the peak C_2 on the SWV of the molten slag. This indicates the amount of the Fe^{3+} ions in the original molten slag is very small under this

condition of experiment. However, Rüssel *et al*[19-21] reported that the reduction peak of Fe^{3+} to Fe^{2+} could be observed on the SWV of a glass melt. This was different from the result obtained in this work. It may be attributed to different atmosphere, melt composition and original iron oxide addition. It should be noted that oxidation of Fe^{2+} in the molten slag was not further defined in the positive potential range because the present work dealt mainly with the reduction of iron ions in the negative potential range.

In order to verify the reduced product in the electrochemical measurement, the molten slags containing 3 wt% FeO were electrolyzed using the Ir wire WE as the cathode for 2 h at constant potentials of -0.40, -1.00, -1.30 V, respectively. Figs. 6 and 7 are respective SEM images and related EDS analyses of the Ir electrode. It can be seen in Fig. 6 that at -0.40 V, no notable change shows at the surface of the Ir electrode. However, when the potential increases to -1.00 V and -1.30 V in the negative direction, a visible loose layer appears at the surface of the Ir electrode. The EDS analyses of the Ir electrode surface as shown in Fig. 7 indicate that when the potential is -0.40 V, no new substance is detectable at the Ir electrode surface. When the potential shifts to -1.00 V, the loose layer at the electrode is identified as a Fe-Ir alloy, indicating deposition of metallic iron in this case. However, there was no evidence for the presence of pure iron at the surface of the electrode. It should also be noted that no dendrite was found. In contrast, iron dendrite could be formed when the iron rod was used as the cathode in a similar previous study.[33] It is reasonable to deduce that the formation of the loose layer as the Fe-Ir alloy is the result of interdiffusion of the deposited Fe and Ir. At -1.30 V, the loose layer at the electrode is a Si-Fe-Ir alloy, indicating co-deposition of iron and silicon. These findings correspond to the results of the reduction peaks appearing in CV and SWV as mentioned above. Therefore, one can judge that the peaks C_1 and C_2 are due to the reduction reactions of $Si^{4+} + 4e \rightarrow Si$ and $Fe^{2+} + 2e \rightarrow Fe$, respectively, and that the electrochemical reduction of Fe^{2+} to Fe occurs in a single two-electron step on the Ir electrode in the molten slag.

In addition, since the loose layer indicates an increase in the area of the electrode contacting molten slag, it can be considered to be a source of capacitance that may explain the increase in the background current in transient electrochemical test. However, the amount of deposited Fe is very small and the time for interdiffusion of Fe and Ir atoms is very short in CV. It can be considered that the increase of the background current (charging current) would be very limited due to a very small increase of the electrode area in this work.

According to the Fe-Ir phase diagram,[55] Fe and Ir can form continuous solid solution alloy at 1723 K. The above SEM images and EDS analyses verify that the reduction product (Fe) of the PE does form the alloy with the Ir electrode. Besides, the morphology of reduction product during the transient process can also be determined by reversal CP.[56,57] Fig. 8 is a current reversal CP curve of the molten slag containing 5 wt% FeO. Three potential plateaus (or shoulders) can be observed. The transition time (τ) associated with the plateau can be determined by the way stated in the literature.[56] It is inferred that the plateau with τ_1 corresponds to Fe^{2+} reduction, the plateau with τ_2 to Fe oxidation, and the plateau with τ_3 to Ir oxidation at more positive potential. In the case of both reactant and product being soluble in solution electrolyte, the ratio of the transition time for oxidation to reduction was reported to be 1/3. The ratio would be unity for the reduction leading to an insoluble deposit on the electrode.[56-59] Here the ratio τ_2/τ_1 is found to be about 1/5.9, indicating the reduction product (Fe) forms a solid solution alloy with the Ir substrate. Further, the smaller τ_2/τ_1 ratio may be caused by relatively slow oxidation of Fe from the alloy electrode.[58] No

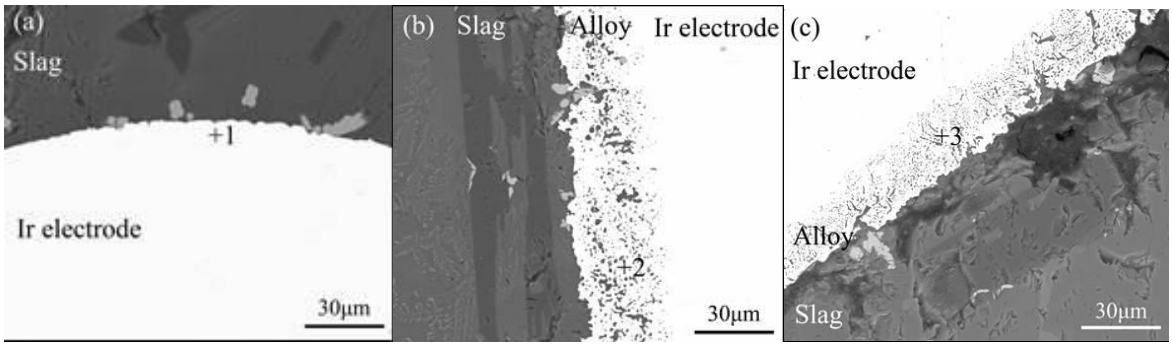

Fig. 6 SEM images of cross (a) and longitudinal (b and c) sections of the Ir electrode recovered from the slag containing 3 wt% FeO after PE for 2 h at -0.40 V (a), -1.00 V (b) and -1.30 V (c). RE: MSZ | Pt | O_2 (air).

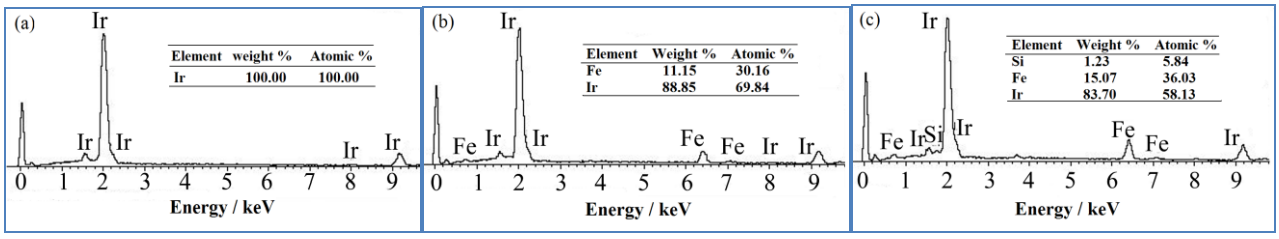

Fig. 7 EDS analyses of spots 1 (a), 2 (b), 3 (c) indicated in **Fig. 6**.

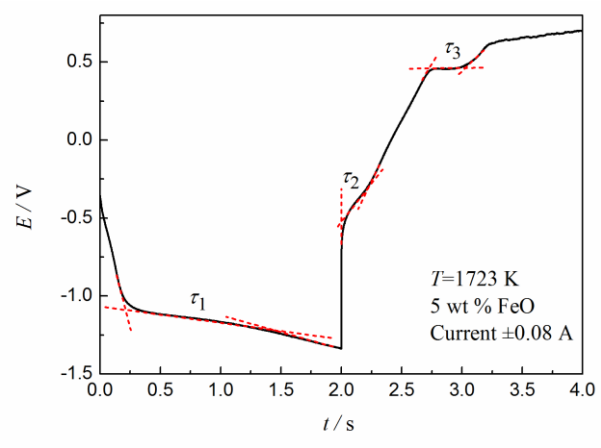

Fig. 8 Reversal CP curve recorded in the molten slag containing 5 wt% FeO at 1723 K. The cathodic and anodic currents are -0.08 and 0.08 A, respectively. RE: MSZ | Pt | O_2 (air)

reduction plateau of Fe^{3+} to Fe^{2+} or O_2 to O^{2-} is found in Fig. 8, indicating that the effect of Fe^{3+} ions or the dissolved oxygen on the reduction of Fe^{2+} ions in the molten slag is insignificant.

Corrosion of MSZ by molten slag. In this work, the key part of the electrolytic cell is the MSZ solid electrolyte tube. It is understandable that the stability of the zirconia based solid electrolyte in the molten slag is a basic necessity to obtain reliable analysis results. According to the literature,[45] calculation with Factsage thermodynamic software suggests that solubility of zirconia in the molten slag containing 5 wt% FeO is only 1.3 wt% at 1723 K under the applied experimental conditions of this work. Note that, this is the result of equilibrium calculation at high temperature for a long time, while the electrochemical transient test lasts usually for a short time. It is reasonable to deduce that the interaction between the MSZ and the molten slag is far from the equilibrium and the amount of zirconia dissolved into the molten slag is very small in this work. Fig. 9 is a typical SEM image showing the cross section at the interface between the MSZ and the slag after an electrochemical test. It is observed that large grains (cubic ZrO_2) still remain in the MSZ (in Fig. 9 small grains denote the monoclinic phase and large

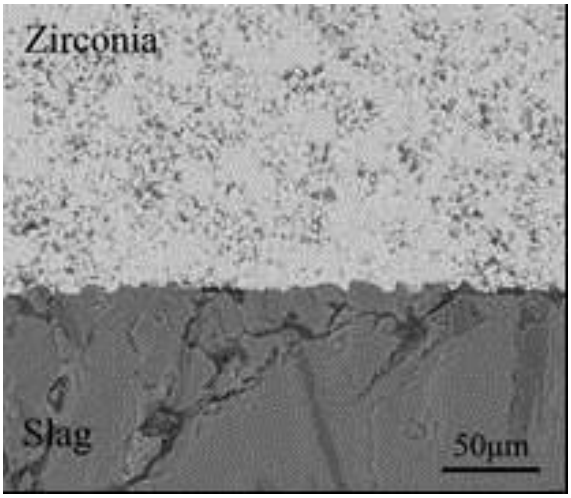

grains the cubic phase, which was confirmed by SEM and EDS in our previous work[33]), and the interface region of the MSZ touching the slag also shows good integrity without any sign of new phase formation or corrosion. Besides, the calculation from the Factsage thermodynamic software shows that the decomposition potential of MSZ is about 2.0 V at 1723 K. So the MSZ cannot be electrolyzed under the conditions of the temperature and the applied potential. Thus it can be concluded that the MSZ tube has sufficiently high stability in the molten slag and the corrosion effect can be neglected. It is feasible to construct the integrated cell using the MSZ tube in this work.

Analyses of electrochemical characteristics of the cell. According to ionic theory, the FeO exists in the forms of Fe^{2+} and O^{2-} in the molten oxide slag which can be considered as an ionic conductor with various cationic carriers such as Ca^{2+}, Mg^{2+}, Fe^{2+} and so on.[60] Thus, the transference number of O^{2-} is small in the molten slag and the transport of O^{2-} is mainly through diffusion. In the MSZ membrane, however, the transference number is close to unity and the O^{2-} movement is mainly through electromigration. Under the condition of the experiment described herein, the current flowing through the cell (or the MSZ membrane) can be considered to be mainly consisting of a pure O^{2-} current (as well as a certain non-faradic charging current).

To enable an electrochemical process in the molten oxide slag with or without FeO, electric neutrality must be maintained in the molten slag. Assuming the absence of oxygen accumulation in the slag, the diffusion flux of O^{2-} in the molten slag must be equal to the electromigration flux of O^{2-} in the MSZ membrane at all times. In the case of scanning in the cathodic direction, electroactive species (ions and/or simple species of elements such as iron, silicon, etc) in the molten slag is apt to reduction or oxidation and produces the corresponding redox peaks. The electromigration flux of O^{2-} (current of oxygen ions) in the MSZ membrane does not increase/decrease with applied potential at all times. Rather, it changes with the reactions of electroactive species. Moreover, the area of the counter electrode (1.26 cm^2) is far larger than that of the working electrode (0.1413 cm^2) in this work. Thus, it can be deemed that the electromigration of O^{2-} in the MSZ membrane will not become the controlling step in the overall reduction process of electroactive species on the Ir electrode. In turn, the electrochemical characteristics of the electroactive species in the molten slag can be reflected by the CVs, SWVs and reversal CP as shown in Figs. 4, 5 and 8, respectively. In addition, by using the zirconia membrane with high oxygen ionic conductivity and low electronic conductivity, the interference of the non-oxide impurities and intrinsic electronic conductivity of the molten slag can be reduced or even eliminated, and that the interactions between the species (particularly oxygen gas) in different electrode solutions can also be prevented. It is well known that the "MSZ | Pt | O_2 (air)" RE has quick response and shows good reversibility, stability and reproducibility.[34,36] The RE in this work can also reflect these characteristics, as shown in Figs. 2 and 9. The obtained regular results indicate that the potential corrosion of MSZ by the molten slag is insignificant to the electrochemical tests. These advantages ensure reliable recording of CV, SWV and CP with high quality in this work.

3.2. Reduction behaviour of Fe^{2+} ions in the molten slag

It is well known that the decisive step in Fe deposition from the molten slag is the reduction of Fe^{2+} ions to Fe. Under the conditions of our experiments, as mentioned earlier, Fe^{2+} is directly added into the slag in the form of ferrous oxalate, the effect of Fe^{3+} on the reduction of Fe^{2+} ions in the molten slag is found to be insignificant although Fe^{3+} can be formed in a small amount by the equilibrium between Fe^{2+}, Fe^{3+} and dissolved oxygen in the molten slag. Therefore, the electroreduction of Fe^{2+} to Fe is the focus of investigation in this work. On the basis of the above analyses, a detailed investigation of the electrochemical reduction of Fe^{2+} ions in the molten slag containing 5 wt% FeO was performed at 1723 K by combining different electrochemical techniques including CV, SWV and CP.

Cyclic voltammetry (CV). Fig. 10 presents CVs recorded at different scan rates in the molten slag containing 5 wt% FeO at 1723 K. These CVs are similar in shape to those in Fig. 4, and dominated by peak C_2 and its anodic counterpart peak A_2. Fig. 10 shows clearly that peak C_2 becomes more negative in potential with increasing the scan rate (v). Considering that *IR* compensation was applied when recording these CVs, the peak potential shift suggests that the reduction of Fe^{2+} ions on the Ir electrode may involve some kinetic complication. On the other hand, the observation of peak A_2 as the anodic counterpart of peak C_2 is evidence that the reduction of Fe^{2+} produces a product that can be reoxidised. To facilitate the subsequent calculation, the peak current (I_p), the peak potential (E_p), the half peak potential ($E_{p/2}$) for C_2 drawn from Fig. 10 are shown in Table 1. The unique shape of CVs in general and the potential shift of the peak C_2 in particular are worth further discussion later on.

The peak current (I_p) can be obtained by deducting the background current from the observed peak current in Fig. 10. Plotting I_p against $v^{1/2}$ in the inset produces a perfect straight line, indicating the reduction of Fe^{2+} ions in the molten slag is diffusion controlled. It can be observed that the fitted straight line in the inset of Fig. 10 does not pass through the origin with a small but positive intercept in the range of applied scan rates. The cause for this non-ideality should not be due to adsorption of the Fe^{2+} ion on the electrode because it is believed that such adsorption should give an intercept on the y-axis first.[11,14,15] Two other probable reasons can be considered. Firstly it may be related to the peak potential shift. The straight line in the inset of Fig. 10 is indication of the diffusion rate being much smaller than the charge transfer rate. These two steps

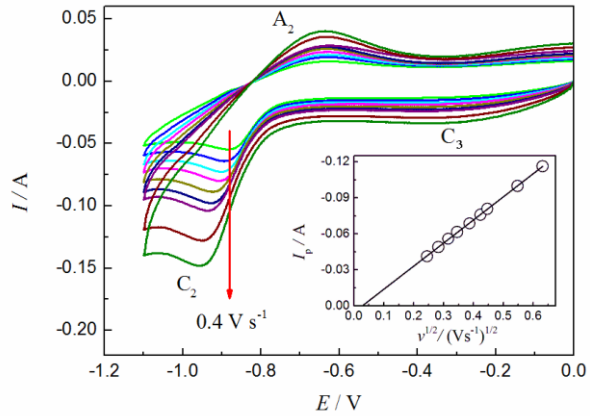

Fig. 10 CVs of molten slag containing 5 wt% FeO with different scan rates (0.06, 0.08, 0.10, 0.12, 0.15, 0.18, 0.20, 0.30, 0.40 V s^{-1}) at 1723 K. Inset: the correlation between cathodic peak current (I_p) and square root of scan rate ($v^{1/2}$). RE: MSZ | Pt | O_2 (air).

differ in that the former is independent of the potential after the peak potential, whilst the latter increases with negatively shifting the potential (or increasing the overpotential). In an ideal case, the peak potential remains the same at different scan rates, so does the charge transfer rate at the peak potential. However, if the peak potential shifts negatively as shown in Fig. 10, the charge transfer rate also increases with increasing the scan rate. This in turn allows a greater diffusion rate and hence a higher current at the peak potential than that in the idea case. Because this effect becomes more significant at higher scan rates, which means the right hand side of the straight line in the inset of Fig. 10 is up-raised from the ideal case. Thus, the extrapolation of the straight line to the left hand side goes below the origin point. It should be noted that the observed peak potential shift may be attributed to several fundamental phenomena such as the following solid solution reaction and the uncompensated electrolyte resistance. This is discussed later in this Section. In addition, the FeO concentration with 5 wt% in the molten slag is on the high side. This may be another reason why the fitted straight line did not pass through the origin with a positive intercept on the x-axis first. Hajasovay[61] also observed the phenomenon with an intercept on the x-axis first when the concentration of electroactive species became high in his work.

Table 1 Results of CV for molten slag containing 5 wt% FeO at 1723 K at different scan rates

Scan rate / V s^{-1}	I_p* / A	E_p / V	$E_{p/2}$ / V	n value from Eq.(3)	n value from Eq.(4)	αn_α value from Eq.(5)
0.06	-0.0413	-0.883	-0.812	4.6	1.6	3.9
0.08	-0.0489	-0.891	-0.821	4.7	1.6	3.9
0.10	-0.0559	-0.900	-0.828	4.5	1.6	3.8
0.12	-0.0615	-0.906	-0.832	4.4	1.5	3.7
0.15	-0.0686	-0.924	-0.842	4.0	1.4	3.4
0.18	-0.0758	-0.926	-0.846	4.1	1.4	3.4
0.20	-0.0807	-0.935	-0.852	3.9	1.4	3.3
0.30	-0.0998	-0.951	-0.861	3.6	1.3	3.1
0.40	-0.1162	-0.953	-0.864	3.7	1.3	3.1

Remark*: The background current has been deducted from the observed peak current in Fig. 10.

The shape of the reduction peak C_2 presents a relatively steep rise and slow decay and it is more pronounced than its re-oxidation counterpart, peak A_2. These features are indicative of part of the reduction product of peak C_2 has been not accessible for oxidation at the applied CV time scale. The Fe-Ir phase diagram[55] shows that no intermetallic compound exists and that there is continuous solid solution alloy in this system at high temperatures. Thus it is believed that the iron produced by the reduction of Fe^{2+} ions in the molten slag dissolves into the Ir electrode and forms a continuous solid solution or alloy. This understanding is in accordance with the earlier reversal CP, SEM images and related EDS analyses of the Ir electrode after PE. The corresponding re-oxidation peak A_2 is broad, which also supports the alloy formation between Fe and Ir during the reduction of the Fe^{2+} ions. Apparently, the activity of the deposited iron in the alloy is lower than that of pure iron, leading to a positive shift for the reduction potential of Fe^{2+} compared with that of Fe^{2+} to pure iron at a given scan rate, which is confirmed by the fact that the onset potential (about -0.70 V) of Fe^{2+} reduction in Fig. 10 is more positive than the decomposition potential (-0.80 V) of the oxide based on the theoretical calculations from Factsage thermodynamics software.

It can be observed that there is a negative shift in the potential of the peak C_2 with increasing the scan rate. This seems to indicate that the electron transfer process is not fully reversible. However, this lower reversibility of iron deposition on the Ir electrode at such a high temperature of 1723 K is quite surprising, because it is expected that the elevated temperature should facilitate surpassing the activation barriers, thus promoting the metal deposition on a solid electrode to be diffusion controlled. As a matter of fact, the presence of re-oxidation peak A_2 in Fig. 10, together with the reverse transition time in Fig. 8, is an indication that the electron transfer process is at least quasi-reversible. On the other hand, it is well known that for a typical quasi-reversible process, the potential of reduction peak usually shifts negatively with increasing the scan rate, while the peak potential of oxidative counterpart shifts positively. However, in this work, it is observed that the potential of the corresponding anodic peak A_2 remains almost constant (indicating re-oxidation of reduction product with a constant activity) irrespective of scan rate. This is inconsistent with typical quasi-reversible characteristics and also seems to indicate the influence of overpotential on the deposition regardless of fast anodic reaction. This phenomenon warrants further discussion.

It should be noted that no cross-over of the current after potential reversal can be seen in Fig. 10, indicating the required nucleation overpotential is negligible and the nucleation does not control the process. It is then possible that the negligible nucleation overpotential results from the formation of an alloy between the deposited iron and the Ir electrode.

As mentioned above, the reduction of Fe^{2+} ions occurs with the formation of the surface alloy. Due to the very small amount of deposited iron during the reduction of Fe^{2+} ions of forward scan, the deposited iron could completely dissolve in a non-saturated state in the abundant Ir substrate. Thus, the activity of deposited iron in the surface alloy is generally smaller than unity (corresponding to the activity of pure solid iron). Nevertheless, the iron activity is larger near the surface than inside the electrode, which results in interdiffusion between the iron atoms from the Ir substrate surface to inside and the iridium atoms in the reverse direction in solid state. Interdiffusion will result in a successive formation of Fe–Ir alloy with a decrease in iron activity. Outwardly the reduction product looks unstable due to interdiffusion. The reduction peak with the formation of the alloy and the interdiffusion process, which is positive of the reversible value obtained in the unperturbed case, shifts in a negative direction (i.e. toward the reversible curve) with increasing scan rate.[62] A higher scan rate indicates the time is short for the initial deposited iron to diffuse into the Ir electrode during the reduction. When the scan rate is high enough, it is likely that there is no time for the deposited iron to diffuse from the surface into the Ir electrode. In other words, the rate of the following interdiffusion is much smaller than that of the charge transfer. In this case the reduction product seems to become stable. Consequently, the difference between reduction and re-oxidation peak potentials would become smaller, which is confirmed by the fact that the three peak potentials observed at the highest scan rates are closer to each other in Fig.10 or Table 1. It can be expected that the reduction of Fe^{2+} to Fe becomes seemingly a reversible process at sufficiently high scan rates. This improved reversibility at higher scan rates is contradictory to a normal reversible electrode reaction. It is known that in CV, many processes are reversible with a constant peak potential at lower scan rates, but may become less reversible at higher scan rates.[63] The so-called reversibility is considered to be abnormal and does not have any significant meaning for an electrode reaction (which will be reflected in the calculation of the number of exchanged electrons later). It can therefore be inferred that the above contradictory in turn supports the effect of the formation of the surface alloy and the following interdiffusion process on a negative shift for the potential of the peak C_2. In other words, alloy formation only complicates the electrode process rather than improves really the reversibility at high scan rates. A detailed discussion on alloy formation will be carried out later.

Furthermore, the higher the scan rate, the larger the current, which can also lead to a distinct potential control error, i.e. the *IR* drop due to the uncompensated resistance. This may be another reason why there is a negative shift in the potential of peak C_2 with increasing the scan rate. Generally there is a certain resistance between the working and the reference electrodes in the cell, which may affect the true potential of the working electrode, especially in the case of a large current.[64] Thus it is necessary to make a compensation for the *IR* drop during testing. However suitable degrees of compensation reported in literatures do not agree with each other.[4,59,64] In this work, the cell was non-conventional and the structure of the molten silicate slag containing iron oxide is also very complex.[65] Thus, a change in the concentration of electroactive species caused by the electrode reaction may have a certain effect on the structure and properties (especially local electrical conductivity and viscosity) of the slag electrolyte in the vicinity of the Ir electrode. The resistance between the working and the reference electrodes, including the resistances of molten slag, is likely not a constant during the electrochemical test. Hence, in theory an appropriate degree of compensation should vary with the progress of the reduction reaction. However, it is very difficult to attain on-line in this work due to the uncertainty of determination of the

compensation resistance. The so-called 100% degree of compensation based on a fixed resistance (about 3 ~ 5 ohms in this work) prior to CV measurement cannot be pronounced as an optimum. Some uncompensated resistance or overcompensation of the *IR* drop always exists during an actual complete measurement. Fig. 11 shows CVs recorded at different compensation degrees for the *IR* drop at the scan rate of 0.2 V s^{-1}. It can be observed that the potential of peak C_2 is constantly shifted towards more positive potentials, whilst that of peak A_2 moved more negatively with increasing the compensation degree from zero (no compensation) to 110%, and no oscillation and deformation on the CV appeared until the compensation degree exceeds 110% (as shown in the inset of Fig. 11). Moreover, the peaks of both C_1 and A_1 even arise with the shift of the peak potential at the compensation degree of 110%. Whilst further investigation is ongoing on the equivalent circuit of the cell to achieve the optimal degree of compensation, it is believed that the compensation degree also has something to do with the scan rate. It can be considered that the compensation is relatively more at lower scan rates and less at higher scan rates under the experimental conditions, which may also result in a slight counterclockwise rotation of the fitted straight line of I_p against $v^{1/2}$ with a positive intercept on the x-axis first in this work. In addition, as mentioned earlier, the potential of the re-oxidation peak A_2 did not shift with increasing the scan rate, a possible explanation is that the compensation for the *IR* drop has become less important due to a smaller reversed current in Fig.10.

As we know, the number of exchanged electrons is an important parameter in the analysis of an electrode process. In a general way, the number of exchanged electrons can be evaluated based on peak potential value from the following general electrochemical formulas which are applicable for a reversible reduction process with soluble-soluble and soluble-insoluble species[66-69] and for irreversible process,[62,70] respectively.

$$E_p - E_{p/2} = -2.2RT/(nF) \quad (3)$$

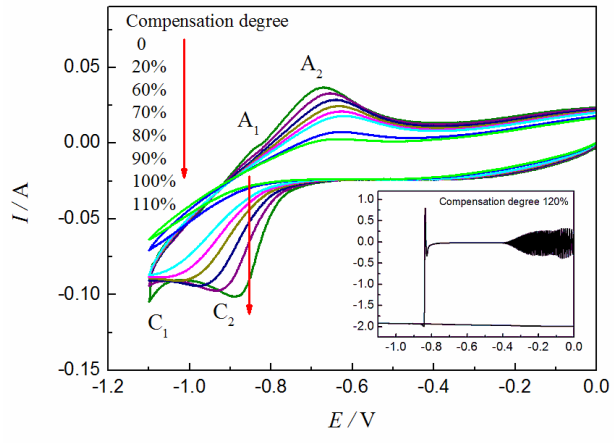

Fig. 11 CVs recorded in molten slag containing 5 wt% FeO with the same scan rate at different *IR* compensation degrees of 0 ~ 110%. Inset: CV recorded at *IR* compensation degree of 120%. Temperature: 1723 K. Scan rate: 0.2 V s^{-1}. RE: MSZ | Pt | O_2 (air).

$$E_p - E_{p/2} = -0.77RT/(nF) \quad (4)$$

$$E_p - E_{p/2} = -1.857RT/(\alpha n_\alpha F) \quad (5)$$

where E_p is the peak potential on a CV (V); $E_{p/2}$ the half peak potential on a CV (V); n the number of exchanged electrons; F the Faraday constant (F = 96500 C mol^{-1}), R the molar gas constant (R = 8.314 J mol^{-1} K^{-1}); T the temperature (K); α the electron transfer coefficient and n_α the number of electrons transferred in the rate determining step. In order to verify the applicability of these formulas in this work, all of them were attempted to calculate the number of electrons since the reversibility of the electron transfer reaction could not be confirmed. It should be noted that the n value corresponding to the reduction peak C_2 has been identified to be 2 as analysed earlier. However, it is found that the n values obtained are between 3.6 and 4.6 from Eq. (3), between 1.6 and 1.3 from Eq. (4), and the values of αn_α are between 3.9 to 3.1 from Eq. (5). These values are also shown in the above Table 1. At various scan rates, the n values are not consistent with the corresponding reduction reaction, and the values of αn_α do not have any significant meaning for an electrode reaction with two-electron transfer since the α value is less than unity. The calculation results show that the correct number of exchanged electrons cannot be obtained based on the peak potential value and all the Eqs. (3) ~ (5) are not really applicable in this work. Obviously, although the formation of the surface alloy and the solid solution reaction are not directly measured by an electrochemical method, they interfere with the observed behaviour and have an effect on the characteristic potentials including the peak potential, leading to invalidation of these general formulas.

Taken together, in this work, the observed potential shift can be attributed to several fundamental phenomena such as the successive formation of surface alloy, the following solid solution reaction involving interdiffusion between Fe and Ir, and the uncompensated electrolyte resistance. These phenomena can distort the electrochemical response and induce the E_p or $E_{p/2}$ to stray beyond the expected values corresponding to reversible electron transfer reaction. It is biased to determine the reversibility of the electron transfer reaction only from the phenomenon that the potential of peak C_2 shifts negatively with increasing the scan rate.

Here, we focus on further analyses of the effects of surface alloying and interdiffusion on the potential. It is know that the successive variation of the activity of deposited iron in the surface alloy inevitably affects the potential during the reduction of Fe^{2+} ions. The iron activity at the surface of the Ir electrode is closely related to the composition of the alloy. However, at present it is very difficult to obtain the quantitative changes of alloy phase composition as a function of parameters during the reduction of Fe^{2+} ions of the forward scan. Nevertheless, it is clear that the composition of the alloy layer on the surface of the Ir electrode depends on three successive fundamental phenomena: electron transfer reaction, surface alloying and intermetallic diffusion. They can be expressed as follows, respectively:

$$Fe^{2+} + 2e \rightarrow Fe \quad (6)$$

$$Fe + Ir \rightarrow Fe\text{-}Ir \text{ (surface alloy)} \quad (7)$$

$$Fe\text{-}Ir \text{ (surface alloy)} \rightarrow Fe\text{-}Ir \text{ (alloy layer)} \quad (8)$$

The first is a heterogeneous electron transfer reaction which can be controlled by the imposed potential. The second is a non-electrochemical alloying process on the electrode surface in which the reduced iron dissolves in the Ir active lattice. The third is also a non-electrochemical solid solution process but due to interdiffusion. Driven by the concentration difference (strictly speaking, chemical potential difference), the last step occurs anyway, and leads to a thermodynamically stable state in the alloy layer, decreasing the activity of deposited iron on the electrode surface. It can be concluded that interdiffusion between Fe and Ir results in the formation of a thin layer of alloy under given conditions. Among the above three steps, the latter two can be regarded as the following coupled process of the former.

When the rate of the first step is far larger than that of the second step, the effect of the latter on the electrode process can be neglected. The apparent electrode process can be described as reaction (6) and the reduced product is treated as pure iron prior to re-oxidation. This is the simplest case and the traditional theories on simple reversible, quasi-reversible and irreversible reactions can be applied for analysis of the mechanism of electrode process. Obviously this is not the case as analysed earlier. When the rate of the first step is far smaller than that of the second step, the electrode process also depends on the reaction (6). However the reduced product exists in the form of alloy due to quick following reaction (7). Thus the apparent electrode process can be described with reaction (9) as follows:

$$Fe^{2+} + Ir + 2e \rightarrow Fe\text{-}Ir \text{ (surface alloy)} \quad (9)$$

The overall reaction scheme for the reduction of Fe^{2+} ions in the molten slag including the above two successive fundamental phenomena may be viewed as the so-called EC process (Here, "E" represents electron transfer reaction (6) and "C" the following surface alloying reaction (7)). Although "C" is a non-electrochemical step, it affects the activity of the product from "E", and hence still has an effect on "E". As mentioned earlier, this is one reason why the onset potential (about -0.7 V) of Fe^{2+} reduction in Fig. 10 is more positive than that of Fe^{2+} to pure iron. It is also possible that the Ir electrode surface loses its local homogeneity due to the deposited iron dissolved heterogeneously in the active Ir lattice. In this case the general electrochemical formulas on reversible or irreversible processes cannot simply be applied for analysis of the mechanism of the electrode process. Similar results have been observed by other researchers in molten slats.[66,71] Unfortunately, this problem is rarely discussed.

The above CVs and reversal CP have shown that the reduction product exists in the continuous solid solution or alloy. Thus, another following interdiffusion process (8) will also go on. The mechanism of electrode process can be further expressed as ECC. Since the layer of the Fe-Ir alloy is successively thickened from the surface to the interior of the Ir electrode, the interdiffusion (8) is considered to be an irreversible process prior to re-oxidation at different scan rates. It is very difficult to give an accurate quantitative analysis because the ECC mechanism is more complex under the conditions of this work. However, the CV does show some important qualitative features of the system.

For examples, as mentioned earlier, the obtained peak current on CVs is proportional to the concentration of Fe^{2+} ions in the molten slag and the square root of scan rate under the conditions of experimentation. Furthermore, in addition to changing the characteristic potential, the following processes are responsible for a smaller re-oxidation current of peak A_2 than the reduction current of peak C_2 as shown by the CVs in Figs. 4 and 10 at the same scan rates. It is well known that the ratio of the anodic to cathodic peak currents should be equal to unity for a reversible reaction with stable reduction product regardless of the scan rate. However, in this work the following interdiffusion process removed part of the reduction product from the electrode surface, which results in a smaller re-oxidation current[65] although exact determination of the re-oxidation peak current is rather difficult, because of uncertainty regarding the choice of the current baseline. The presence of the following interdiffusion process can also be confirmed by the fact that the ratio τ_2/τ_1 in Fig. 8 is 1/5.9 rather than general 1/3 based on a reduction product dissolved in the molten electrolyte. It should be mentioned that the rate of diffusion of Fe in the solid Ir phase is not comparable to the rate of diffusion of Fe^{2+} ions in the molten slag phase. Consequently, the occurrence of the following interdiffusion process should, at most, reduce the anodic peak current but should never remove it.

Square wave voltammetry (SWV). A further investigation was made using the SWV technique. SWVs from the molten slag containing 5 wt% FeO is shown in Fig. 12. It can be observed that the peak C_2 exhibits a basically symmetrical signal, which may be attributed to negligible nucleation overpotential due to the formation of alloy phase. The potential of peak C_2 is basically in the same range as that in Fig. 10 and hardly shifts with increasing the frequency (f), while that of peak C_3 shifts evidently to more negative potentials. By plotting peak current (I_p) against $f^{1/2}$ for the peak C_2 in Fig. 12, a favourable linear relation is obtained as shown in inset of Fig. 12. However, this linear relation does not necessarily mean the reduction of Fe^{2+} to be reversible because the number of exchanged electrons as calculated[56,57,59,47,73] from the following Eq. (10) ranged between 4 and 6 based on the peak C_2 in Fig. 12, which is also

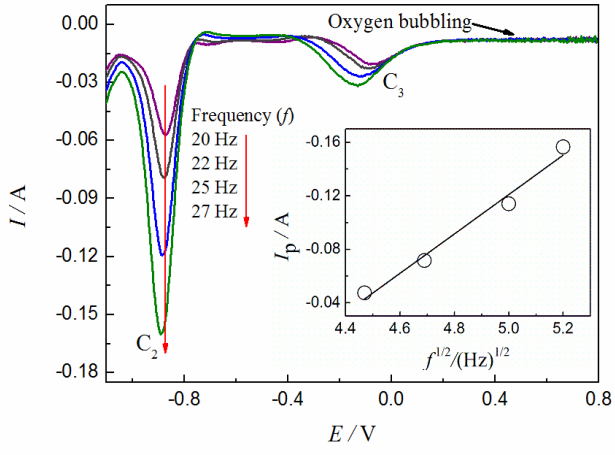

Fig. 12 SWV curves for molten slag containing 5 wt% FeO with different frequency values of 20, 22, 25, 27 Hz at 1723 K. Inset: the correlation between the current (I_p) of cathodic peak C_2 and square root of the frequency ($f^{1/2}$). RE: MSZ | Pt | O_2 (air).

inconsistent with the corresponding reaction. It is believed the cause of this phenomenon is the same as for the above inapplicable equations due to surface alloying and interdiffusion. Chryssoulakis *et al*[12] attributed it to partial solubility of iron in platinum electrode in their work.

$$W_{1/2} = 3.52RT/(nF) \quad (10)$$

where $W_{1/2}$ is the half-peak width (V).

It is also notable in Fig. 12 that the measured current prior to peak C_3 is slightly disturbed by oxygen bubbling at a more anodic potential. Disturbance amplitude decreases with the scan from anodic to cathodic potential, indicating the amount of oxygen molecules in the molten slag decreased. This is a more visible indication that the peak C_3 is associated to the reduction of oxygen molecules to free oxygen ions. However, the peak C_3 does not appear on the CVs recorded in the blank slag. It was reported[49,73] that the solubility of oxygen gas in a molten slag may increase by addition of the so-called network modifier oxide. The FeO can be considered as a network modifier oxide, and the solubility of oxygen gas in molten slag containing FeO is expected to be larger than that in the blank slag. It is thus understandable that the peak C_3 appears on the SWVs of FeO containing molten slags but not on the CV of the blank slag. No visible reduction peak of Fe^{3+} is observed, which is consistent with the earlier view of neglecting Fe^{3+} ions.

Chronopotentiometry (CP). CP was also employed to investigate the Fe^{2+} reduction process. Fig. 13 presents CP curves recorded on the Ir electrode in the molten slag containing 5 wt% FeO. Two potential plateaus are observed, of which the first one appears at about -1.0 ~ -1.2 V, indicating the Fe^{2+} reduction, and then it transits to the Si^{4+} reduction at more negative potentials. No sign for reduction of Fe^{3+} or O_2 is observed on the CP curves, which is consistent with the earlier observation (as shown in Fig. 8). Comparing with CVs or SWVs, the potentials of the plateaus for Fe^{2+} and Si^{4+} reduction on the CP curves shift negatively with increasing the cathodic current. This is because the *IR* drop compensation is applied between working and reference electrodes for recording CV or SWV, whilst no *IR* drop compensation is applied for recording CP.

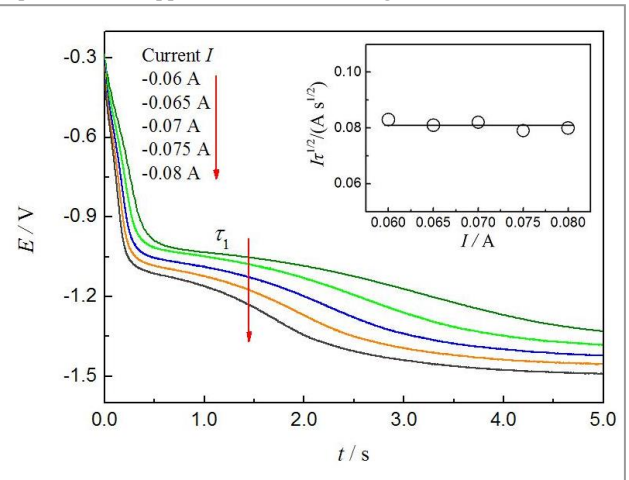

Fig. 13 CP curves recorded at different cathodic currents in the slag containing 5 wt% FeO at 1723 K. Inset: the correlation between cathodic current *I* and $I\tau^{1/2}$ (τ: transition time) for the first plateau. RE: MSZ | Pt | O_2 (air).

The inset of Fig. 13 is $I - I\tau^{1/2}$ plot for the first plateau. It shows that the $I\tau^{1/2}$ value on CP curves is basically unchanged with the variation of *I*. This indicates that the currents are high enough to place the reactions of Fe^{2+} ions reduction on the Ir electrode from the molten slag in a diffusion controlled region.[57,74,75] Then, the diffusion coefficient of the Fe^{2+} ions can be derived from Sand's Equation[75], i.e. Eq. (11), as follow:

$$I = 1/2\pi^{1/2} nFAD^{1/2} C_0 \tau^{-1/2} \quad (11)$$

where *I* is applied cathodic current (A); τ transition time (s); *A* the area of working electrode (A = 0.1413 cm^2), C_0 the molarity of the electroactive Fe^{2+} ion (it can be calculated to be 1.81×10^{-3} mol cm^{-3} from the density of molten slag obtained in the literature[76]). *D* the diffusion coefficient of the Fe^{2+} ion ($cm^2\ s^{-1}$). It should be noted that the application of Sand's Equation is not dependent on the reversibility of reaction.[77]

The diffusion coefficient value of Fe^{2+} is derived to be D = (3.43±0.06) × 10^{-6} $cm^2\ s^{-1}$ from Eq. (11). To our knowledge, the limited literature data on diffusion coefficient values of Fe^{2+} ions are 1.3×10^{-6} $cm^2\ s^{-1}$ in a molten slag of 39.44 wt% CaO, 39.44 wt% SiO_2,19.71 wt% Al_2O_3, and 1.41 wt% FeO at 1573 K,[18] 8.07×10^{-6} $cm^2\ s^{-1}$ in 29.79 wt% CaO, 31.91 wt% SiO_2 and 38.30 wt% FeO at 1723 K,[78] and (2.1 ~ 5.0)$\times10^{-6}$ $cm^2\ s^{-1}$ in 43 wt% CaO, 35wt % SiO_2 and 22 wt% Al_2O_3 at 1773 K,[79] respectively. Taking into account the differences in slag composition, temperature and measurement method, the diffusion coefficient value obtained in this work is in a good agreement with those reported values in the above literatures, indicating the reasonablity of the Eq. (11) for investigating Fe^{2+}/Fe couple in this work.

4. Conclusions

A unique integrated three-electrode cell with the "MSZ | Pt | O_2 (air)" RE was constructed using an MgO-stabilised zirconia based solid electrolyte tube, electrochemical behaviour of iron ions was systematically investigated on an Ir WE in SiO_2-CaO-MgO-Al_2O_3 molten slag at a high temperature of 1723 K. The test results show that the electromigration of O^{2-} ions in the MSZ tube does not become the controlling step in the overall reduction process of electroactive species on the electrode and it is feasible to investigate electrochemical behaviour of iron ions in the molten slag with the aid of the integrated cell.

By combining different electrochemical techniques (i.e. CV, SWV, CP and PE), it is concluded that the electrochemical reduction of Fe^{2+} to Fe on the Ir electrode in the molten slag follows a single two-electron transfer step, and the rate of the process is diffusion controlled. The obtained peak current in CVs is proportional to the concentration of Fe^{2+} ions in the molten slag and the square root of scan rate. However, several following coupled processes such as the formation of surface alloy and interdiffusion process can affect the kinetics of the deposition process. The ECC mechanism was proposed to explain the CV observations. The diffusion coefficient value of Fe^{2+} ions in the molten slag containing 5 wt% FeO at 1723 K have been derived based on CP curves. Meanwhile, iron alloys

can be produced from the molten slag containing FeO, although the ultimate aim of this research is the production of pure iron which in real industrial electrolysis may not necessarily use the integrated cell.

Acknowledgements

The authors acknowledge funding provided by the National Natural Science Foundation of China (Grant No.51174148) and the Key Program of Joint Funds of the National Natural Science Foundation of China and the Government of Liaoning Province (Grant No. U1508214).

References

1 W.Q. Sun, J.J Cai, H.J. Mao and D.J. Guan, *J. Iron Steel Res. Int.*, 2011, **18**, 31-36.
2 S. Jahanshahi, J. G. Mathieson and H. Reimink, *J. Sustain. Metall.*, 2016, **2**, 185-190.
3 A. Allanore, L. Yin and D.R. Sadoway, *Nature*, 2013, **497**, 353-356.
4 D.H. Wang, A.J. Gmitter and D.R. Sadoway, *J. Electrochem. Soc.*, 2011, **158**, E51-E54.
5 A.H.C. Sirk, D.R. Sadoway and L. Sibille, *ECS. Trans.*, 2010, **28**(6), 367-373.
6 A. Allanore, *Electrochim. Acta*, 2013, **110**, 587-592.
7 A. Allanore, *J. Electrochem. Soc.*, 2015, **162**, E13-E22.
8 G.M. Haarberg, E. Kvalheim, S. Rolseth, T. Murakami, S. Pietrzyk and S. Wan, *ECS. Trans.*, 2007, **3**(35), 341-345.
9 N.M. Ferreira, A.V. Kovalevsky, M.C. Ferro, F.M. Costa and J.R. Frade, *Ceram. Inter.*, 2016, **42**, 11070-11076.
10 M. Barati and K.S. Coley, *Metall. Mater. Trans. B*, 2006, **37**, 41-49.
11 S.Z. Duan, P. Dudley and D. Inman, *J. Electroanal. Chem.*, 1982, **142**, 215-228.
12 J. Chryssoulakis, J. Bouteillon and J.C. Poignet, *J. Appl. Electrochem.*, 1978, **8**, 103-108.
13 Y. Castrillejo, A.M. Martínez, M. Vega and E. Barrado, *J. Electroanal. Chem.*, 1995, **397**, 139-147.
14 A. Lugovskoy, M. Zinigrad, D. Aurbach and Z. Unger, *Electrochim. Acta*, 2009, **54**, 1904-1908.
15 C. Donath, E. Neacsu and N. Ene, *Rev. Roum. Chim.*, 2011, **56**, 763-769.
16 M. Nakashima, H. Yamashita and T. Maekawa, *J. Non-Cryst. Solids*, 1998, **223**, 133-140.
17 J.D. Strycker, P. Westbroek and E. Temmerman, *J. Electroanal. Chem.*, 2004, **565**, 149-158.
18 K. Nagata, T. Kawashima and K.S. Goto, *ISIJ Int.*, 1992, **32**, 36-42.
19 C. Rüssel and A. Wiedenroth, *Chem. Geol.*, 2004, **213**, 125-135.
20 A. Wiedenroth and C. Rüssel, *J. Non-Cryst. Solids*, 2003, **320**, 238-245.
21 T. Sugawara, Y. Fujita, M. Kato, S. Yoshida, J. Matsuoka and Y. Miura, *J. Ceram. Soc. Jpn.*, 2009, **117**, 1317-1323.
22 E. Franks, *J. Appl. Electrochem.*, 1977, **7**, 147-151.
23 D.J. Fray, *Metall. Mat. Trans. B*, 2003, **34**, 589-594.
24 M.J.U.T. Van Wijngaarden, R.J. Dippenaar and P.M. Van Den Heever, *J. S. Afr. Inst. Min. Metall.*, 1987, **87**, 269-278.
25 Y.M. Gao, J.X. Song, Y.Q. Zhang and X.M. Guo, *Acta Metall. Sin.*, 2010, **46**, 277-281.
26 R. Ganesan, T. Gnanasekaran and R.S. Srinivasa, *J. Nucl. Mater.*, 2006, **349**, 133-149.
27 T. Ogura, R. Fujiwara, R. Mochizuki, Y. Kawamoto, T. Oishi and M. Iwase, *Metall. Trans. B*, 1992, **23**, 459-466.
28 E.T. Turkdogan, *Ironmaking Steelmaking*, 2000, **27**, 32-36.
29 P. Soral, U. Pal, H.R. Larson and B. Schroeder, *Metall. Mat. Trans. B*, 1999, **30**, 307-321.
30 W. Kim, D.J. Min, Y.S. Lee and J.H. Park, *ISIJ Int.*, 2009, **49**, 1882-1888.
31 X. Guan, S. Su，U.B. Pal and A.C. Powell, *Metall. Mat. Trans. B*, 2014, **45**, 2138-2144.
32 E.S. Gratz, X. Guan, J.D. Milshtein, U.B. Pal and A.C. Powell, *Metall. Mat. Trans. B*, 2014, **45**, 1325-1336.
33 Y.M Gao, C. Duan, Y.B. Yang, D. Ruan, C.H. Yang and C. Hong, , *ISIJ Int.*, 2015, **55**, 2273-2282.
34 C. Mallika, O.M. Sreedharan and R. Subasri, *J. Eur. Ceram. Soc.*, 2000, **20**, 2297-2313.
35 S.C. Britten and U.B. Pal, *Metall. Mater. Trans. B*, 2000, **31**, 733-753.
36 C.Z. Wang, Solid Electrolyte and Chemical Sensors, Metallurgical Industry Press, Beijing, 2000.
37 L. Hong, M. Hirasawa, S. Yamada and M. Sano, *ISIJ Int.*, 1996, **36**, 1237-1244.
38 K.R. Lee and H. Suito, *Metall. Mat. Trans. B*, 1994, **25**, 893-902.
39 Y. Kang, K. Nomura, K. Tokumitsu, H. Tobo and K. Morita, *Metall. Mat. Trans. B*, 2012, **43**, 1420-1426.
40 S. Jahanshahi and S. Wright, *ISIJ Int.*, 1993, **33**, 195-203.
41 H. Ohta and H. Suito, *Metall. Mat. Trans. B*, 1998, **29**, 119-129.
42 S.L. Teasdale and P. C. Hayes, *ISIJ Int.*, 2005, **45**, 634-641.
43 A.J. Gmitter, The influence of inert anode material and electrolyte composition on the electrochemical production of oxygen from molten oxides, Massachusetts Institute of Technology, Cambridge, 2008.
44 http://www.factsage.com/, (accessed March 20 2017)
45 M.O. Suk and J.H. Park, *J. Amer. Ceram. Soc.*, 2009, **92**, 717-723.
46 H. Okamoto, *JPED*, 2007, **28**, 495.
47 A. Osipenko, A. Maershin, V. Smolenski, A. Novoselova, M. Kormilitsyn and A. Bychkov, *J. Electroanal. Chem.*, 2011, **651**, 67-71.
48 R. Prange, K. Heusler and K. Schwerdtfeger, *Metall. Trans. B*, 1984, **15**, 281-288.
49 M. Sasabe and K.S. Goto, *Metall. Trans.*, 1974, **5**, 2225-2233.
50 L.X. Yang and G.R. Belton, *Metall. Mat. Trans. B*, 1998, **29**, 837-845.
51 M.D. Dolan and R.F. Johnston, *Metall. Mater. Trans. B*, 2004, **35**, 675-684.
52 D.J. Min and R.J. Fruehan, *Metall. Mater. Trans. B*, 1992, **23**, 29-37.
53 A.A. Borisov, *Petrology*, 2010, **18**, 471-481.

54 J. Di Martino, C. Rapin, P. Berthod, R. Podor and P. Steinmetz, *Corrosion Science*, 2004, **46**, 1849-1864.
55 L.J. Swartzendruber, *Bulletin of Alloy Phase Diagrams*, 1984, **5**, 48.
56 L. Massot, P. Chamelot and P. Taxil, *Electrochim. Acta*, 2005, **50**, 5510-5517.
57 C. Hamel, P. Chamelot and P. Taxil, *Electrochim. Acta*, 2004, **49**, 4467-4476.
58 M. Jayakumar, K.A. Venkatesan and T.G. Srinivasan, *Electrochim. Acta*, 2008, **53**, 2794-2801.
59 H. Tang and B. Pesic, *Electrochimica. Acta*, 2014, **119**, 120-130.
60 K.S. Goto, A review of the electrolytic properties of metallurgical slags, IN proceedings of the 2nd International Symposium on Metallurgical Slags and Fluxes, Lake Tahoe NV, November, 1984, 839-862.
61 J. Hajasova, Electrochemical behaviour of sulphur containing species in molten salts, Norwegian University of Science and Technology, Trondheim, 2007.
62 A.J. Bard and L. R. Faulkner, *Electrochemical Methods Fundamentals and Applications*, 2nd Ed., John Wiley & Sons, Inc, New York, 2001, 236-239.
63 A.J. Bard and L.R. Faulkner, *Electrochemical Methods Fundamentals and Applications*, 2nd Ed., John Wiley & Sons, Inc, New York, 2001, 470-521.
64 A.J. Bard and L.R. Faulkner, *Electrochemical Methods Fundamentals and Applications*, 2nd Ed., John Wiley & Sons, Inc, New York, 2001, 645-650.
65 B.O. Mysen, F. Seifert and D. Virgo, *Am. Mineral.*, 1980, **65**, 867-884.
66 S. Vandarkuzhali, M. Chandra, S. Ghosh, N. Samanta, S. Nedumaran, B. Prabhakara Reddy and K. Nagarajan, *Electrochim. Acta*, 2014, **145**, 86-98.
67 B.P. Reddy, S. Vandarkuzhali, T. Subramanian and P. Venkatesh, *Electrochim. Acta*, 2004, **49**, 2471-2478.
68 R.S. Nicholson and I. Shain, *Anal. Chem.*, 1964, **36**, 706-723.
69 G. Mamantov, D.L. Manning and J.M. Dale, *J. Electroanal. Chem.*, 1965, **9**, 253-259.
70 H. Matsuda and Y. Ayabe, *Z. Elektrochem*, 1955, **59**, 494-503.
71 J. Kaufmann and C. Rüssel, *J. Non-Cryst. Solids*, 2008, **354**, 4614-4619.
72 C. Nourry, P. Souček, L. Massot, R. Malmbeck, P. Chamelot and J.P. Glatz, *J. Nucl. Mater.*, 2012, **430**, 58-63.
73 M. Sasabe and Y. Kinoshita, *Trans. ISIJ*, 1980, **20**, 801-809.
74 C.S. Wang, Y. Liu and H. Hi, *J. Rare. Earth.*, 2013, **31**, 405-409.
75 A.J. Bard and L.R. Faulkner, *Electrochemical Methods Fundamentals and Applications*, 2nd Ed., John Wiley & Sons, Inc, New York, 2001, 307-316.
76 J.X. Chen, *Common Chart Data Handbook in Steelmaking*, Metallurgical Industry Press, Beijing, 1984.
77 H. Tang and B. Pesic, *Electrochim. Acta*, 2014, **133**, 224-232.
78 D.P. Agarwal and D.R. Gaskell, *Metall. Trans. B*, 1975, **6**, 263-267.
79 J.Y. Zhang, *Physical Chemistry of Metallurgy*, Metallurgical Industry Press, Beijing, 2004.